



This is the accepted manuscript made available via CHORUS. The article has been published as:

Magnetic anisotropy of ferromagnetic $\text{Ga}_{1-x}\text{Mn}_x/\text{As}_{1-y}\text{P}_y$ films with graded composition

Seul-Ki Bac, Sanghoon Lee, Xinyu Liu, Malgorzata Dobrowolska, Badih A. Assaf, and Jacek K. Furdyna

Phys. Rev. Materials **5**, 054414 — Published 28 May 2021

DOI: [10.1103/PhysRevMaterials.5.054414](https://doi.org/10.1103/PhysRevMaterials.5.054414)

Magnetic Anisotropy of Ferromagnetic $\text{Ga}_{1-x}\text{Mn}_x\text{As}_{1-y}\text{P}_y$ Films with Graded Composition

Seul-Ki Bac^{1,2*}, Sanghoon Lee^{1†}, Xinyu Liu², Malgorzata Dobrowolska², Badih A. Assaf², and Jacek K. Furdyna²

¹Department of Physics, Korea University, Seoul 02841, Republic of Korea

²Department of Physics, University of Notre Dame, Notre Dame, IN 46556, U. S. A.

Abstract

We have investigated magnetic anisotropy properties of ferromagnetic semiconductor $\text{Ga}_{1-x}\text{Mn}_x\text{As}_{1-y}\text{P}_y$ films grown by molecular beam epitaxy on GaAs substrates with constant Mn content x of 0.06, and with P content y graded along the growth direction. Two samples were investigated, one with y increasing in the growth direction from 0.03 to 0.24, the other with y decreasing from 0.25 to 0.04. Such grading of phosphorus concentration leads to a continuous variation of strain, and thus of magnetic anisotropy in the film. Although the phosphorus mole fraction in the films was varied by nearly the same amount in both ‘forward’- and ‘reverse’-graded samples, their magnetic anisotropy properties are entirely different. Specifically, while the ‘forward’-graded specimen can be described in terms of three distinct magnetic layers in which the magnetic easy axes progress from in-plane to out-of-plane as the phosphorus concentration increases, the ‘reverse’-graded sample shows only an out-of-plane anisotropy throughout the entire film. This implies that the initial conditions at the nucleation of sample growth determine the magnetic properties of the entire graded $\text{Ga}_{1-x}\text{Mn}_x\text{As}_{1-y}\text{P}_y$ film.

* Corresponding author: sbac@nd.edu

† Corresponding author: slee3@korea.ac.kr

I. INTRODUCTION

Over the past two decades, diluted magnetic semiconductor alloys $\text{Ga}_{1-x}\text{Mn}_x\text{As}$ have received attention as promising candidates for spintronic applications [1,2]. It is now well established that ferromagnetism in these alloys originates from exchange interactions between the spins of magnetic ions and itinerant holes [3]. This spin-carrier interplay offers remarkable features, such as a strong dependence of the Curie temperature on carrier density and a strong sensitivity of magnetic anisotropy of these alloys to epitaxial strains related to the strain-dependent anisotropy of the valence band [3,4]. Usually, when the $\text{Ga}_{1-x}\text{Mn}_x\text{As}$ layers are under compressive strain (as in the case when they are grown on GaAs substrates), this situation favors in-plane magnetization [5]. On the contrary, when the $\text{Ga}_{1-x}\text{Mn}_x\text{As}$ layers are under tensile strain, the magnetization of the layer orients spontaneously perpendicular to the film plane, as in the case of $\text{Ga}_{1-x}\text{Mn}_x\text{As}$ films grown on $\text{Ga}_{1-x}\text{In}_x\text{As}$ buffer layers [6], or when a sufficient concentration of phosphorus is incorporated into the $\text{Ga}_{1-x}\text{Mn}_x\text{As}$ lattice [7,8]. Thus, quaternary $\text{Ga}_{1-x}\text{Mn}_x\text{As}_{1-y}\text{P}_y$ alloys provide a powerful approach for tailoring magneto-crystalline anisotropy by controlling the concentration of P in the film [9,10].

Interfacial effects have been ubiquitously employed to induce symmetry breaking and perform band engineering in semiconductors [11-13]. One method to introduce and enhance such interfacial effects utilizes a composition gradient during the synthesis of semiconductors to tune strain and band structure [14]. In the present work, we studied magnetic anisotropy in $\text{Ga}_{1-x}\text{Mn}_x\text{As}_{1-y}\text{P}_y$ samples in which the concentration of P is graded along with the film thickness, with Mn concentration kept at a constant value of $x \approx 0.06$. In such films, the graded phosphorus concentration is expected to lead to a gradient of the energy gap (and thus of the hole concentration, which mediates the Mn-Mn exchange coupling) and a gradient of strain (and thus of magnetic anisotropy parameters). One can then expect in such graded specimens an entirely new magnetic behavior with novel ferromagnetic properties. In fact, in our earlier studies of such graded systems [15,16], some of the authors have already found a pronounced and unique

1 asymmetry of domain walls with respect to their easy axes, suggesting the presence of Dzyaloshinskii-
2 Moriya interactions and novel programmable magnetic bias effects.

3 Importantly, the variation of magnetic anisotropy in the graded film can realize a monolithic
4 ferromagnetic structure comprised of multiple magnetic sublayers with in-plane and out-of-plane
5 components of magnetization, which is a candidate system for field-free spin-orbit torque switching [17-
6 19]. Detailed investigation of magnetic anisotropy in the graded $\text{Ga}_{1-x}\text{Mn}_x\text{As}_{1-y}\text{P}_y$ films is also likely to shed
7 light on the importance of initial nucleation mechanism during crystal growth, which is closely related to
8 crystallinity, composition, and defect formation [20,21], and can thus provide fruitful information for
9 optimizing structures for spintronic device applications.

11 II. EXPERIMENTS

12 Composition-graded $\text{Ga}_{1-x}\text{Mn}_x\text{As}_{1-y}\text{P}_y$ samples were grown on GaAs (001) substrates in a Riber 32
13 molecular beam epitaxy (MBE) system. During the growth, wafers were rotated to achieve a homogeneous
14 composition in the film plane. For grading the P concentration, the $\text{As}_2/(\text{Ga}, \text{Mn})$ flux ratio was kept
15 constant at ~ 10 during the entire growth, while the P_2/As_2 ratio was gradually varied during the growth. In
16 one sample (referred to as the ‘forward’ sample), the P_2/As_2 flux ratio was increased from ~ 0 to $\sim 1/2$, and
17 in the second sample (referred to as ‘reverse’), the P_2/As_2 ratio was reduced from $\sim 1/2$ to ~ 0 as the growth
18 progressed. Such gradation of the flux ratio during growth resulted in $\text{Ga}_{1-x}\text{Mn}_x\text{As}_{1-y}\text{P}_y$ films in which y
19 changes continuously either from 0.03 to 0.24 (the ‘forward’ sample) or from 0.25 to 0.04 (the ‘reverse’
20 sample) at a fixed value of $x \approx 0.06$. The atomic concentrations in both samples were examined by high-
21 resolution x-ray diffraction (XRD) measurements, as described in Ref. [16]. The thicknesses of the ‘forward’
22 and ‘reverse’ samples were determined by the XRD data (see Fig. S1 in [22]) as 103 ± 1.8 nm and 63 ± 1.1
23 nm, respectively. Despite the variation of phosphorous concentrations, both samples were fully strained
24 with no detectable relaxation (see Fig. S2 in [22]). Schematic cross-sections of the graded $\text{Ga}_{1-x}\text{Mn}_x\text{As}_{1-y}\text{P}_y$
25 films used in this investigation are shown in Figs. 1(a) and 1(b).

1 For electrical transport measurements, Hall bars were patterned by photolithography and dry etching,
 2 with the long direction along with the [110] crystalline orientation. A schematic image of the Hall device
 3 is shown in Fig. 1(c). Directions of the applied magnetic field and of magnetization in the films are indicated
 4 by angles (φ_H, θ_H) and (φ, θ) , respectively, with the polar angles θ_H and θ measured from the [001]
 5 crystallographic direction, and the azimuthal angles φ_H and φ from the [110] direction (which is also the
 6 direction of the current), as shown in Fig. 1(c). The temperature dependence of resistance shown in Fig.
 7 1(d) provides an estimate of Curie temperatures of the ‘forward’ sample as 40 K and the ‘reverse’ sample
 8 as 65 K. These agree well with the results obtained from the temperature dependence of R_{xy}/R_{xx}^2 extracted
 9 from Arrott plots (see Section II in [22]).

11 III. RESULTS

12 In this study, we will use Hall effect measurements for determining the magnetic anisotropy of our
 13 graded specimens. We recall that the expression for Hall resistance in a ferromagnetic film is given by [1,23]

$$14 \quad R_{xy} = R_0 \frac{H}{t} \cos \theta_H + R_S \frac{M}{t} \cos \theta + k \frac{M^2}{t} \sin^2 \theta \sin 2\varphi, \quad (1)$$

15 where the first, second, and third terms on the right-hand side of Eq. (1) are the normal, anomalous, and
 16 planar Hall resistances, respectively. The terms R_0 and R_S are the normal and anomalous Hall coefficients,
 17 k is a constant related to the anisotropic magnetoresistance of the sample, and M and t are its magnetization
 18 and thickness. The anomalous and planar Hall resistances depend directly on the orientation of
 19 magnetization, which thus provide a convenient tool for determining the magnetic anisotropy of the film.

21 A. Magnetic anisotropy of ‘forward’-graded Sample

22 Field dependences of the Hall resistances R_{xy} of our graded $\text{Ga}_{1-x}\text{Mn}_x\text{As}_{1-y}\text{P}_y$ samples measured at
 23 10 K are shown in Fig. 2. Because the strain in the samples is graded, it is reasonable to expect that different
 24 sample sections may be characterized by in-plane and out-of-plane easy axes. This is clearly confirmed by

1 the out-of-plane field scans of the ‘forward’ sample shown in Fig. 2(b), in which a fraction of the R_{xy} signal
 2 (of magnitude marked as R_{cent}^{OP} in the figure) shows a distinct sharp hysteresis loop in the low-field region,
 3 indicating that a fraction of that sample has an out-of-plane easy axis. However, as the field increases
 4 beyond the central hysteresis, R_{xy} continues to increase at a gradual rate. Since a portion of the sample with
 5 low phosphorus content is expected to have an in-plane easy axis, we ascribe the observed gradual increase
 6 of R_{xy} to magnetization from that portion being “forced” normal to the sample plane by the out-of-plane
 7 field until the entire magnetization of the graded film aligns with the applied out-of-plane field, thus
 8 providing a measure of total magnetization, marked in Fig. 2(b) as R_{tot}^{OP} .

9 Figure 2(a) shows R_{xy} for the ‘forward’ sample obtained with the applied field scanned in the film
 10 plane (in this case at $\theta_H = 90^\circ$, $\varphi_H \sim 100^\circ$), showing a two-step switching behavior that is typically
 11 observed in planar Hall effect (PHE) measurements on the $\text{Ga}_{1-x}\text{Mn}_x\text{As}$ films with two in-plane magnetic
 12 easy axes [24]. Importantly, however, the present results also show a small vertical shift between the up-
 13 and down-sweeps of the field, marked as R_{asym}^{IP} in Fig. 2(a). Such vertical shift of Hall resistance cannot
 14 be caused by the in-plane magnetic anisotropy of the layer and must be ascribed to a small contribution
 15 from the anomalous Hall effect (AHE) [25,26]. This can be explained by the fact that, although the data in
 16 Fig. 2(a) are obtained with the field applied in the film plane, a slight misalignment of that field with the
 17 layer plane is inevitable, resulting in the presence of a weak but finite out-of-plane field component. Such
 18 out-of-plane component of the applied field will then align the magnetization from the sample fraction
 19 having an out-of-plane easy axis (as identified in our discussion of Fig. 2(b)) normal to the film, resulting
 20 in the AHE contribution to R_{xy} , and thus in the observed shift marked as R_{asym}^{IP} . The two features observed
 21 around 600 G in Fig. 2(b) can thus be understood as resulting from such slight field misalignment, which
 22 introduces an admixture of PHE into the R_{xy} data in Fig. 2(b), and thus an admixture of the steps associated
 23 with in-plane reorientations of magnetization seen in Fig. 2(a). Note, however, that the steps corresponding
 24 to these reorientations in Fig. 2(b) occur at fields much higher than in Fig. 2(a), since now a much higher

1 field must be applied before the in-plane field component reaches the value required for such reorientations.
2 The misalignment angle can be estimated from the difference of switching fields for the two measurements
3 shown in Figs. 2(c) and 2(d), which give 4° as the upper end of the deviation angle.

4 Having established the origin of the asymmetry marked as R_{asym}^{IP} in Fig. 2(a), and defining R_{cent}^{OP}
5 and R_{tot}^{OP} in Fig. 2(b) that indicate, respectively, the contributions to AHE of the magnetization of the layer
6 with an out-of-plane easy axis and the total (i.e., saturated) magnetization, we can now estimate the fractions
7 of the ‘forward’ sample characterized by in-plane and out-of-plane easy axes. In the out-of-plane
8 measurements shown in Fig. 2(b), the ratio of $R_{cent}^{OP}/R_{tot}^{OP}$, indicating the fraction of the sample with an out-
9 of-plane easy axis to the total sample magnetization, is approximately 20 %. Similarly, the contribution of
10 the out-of-plane magnetization to the planar Hall resistance shown in Fig. 2(a) can be calculated from
11 R_{asym}^{IP} , since, as argued above, that represents the AHE contribution to R_{xy} in the in-plane measurement.
12 The value of $R_{asym}^{IP}/R_{tot}^{OP} \approx 0.1$, indicating that approximately 10% of the sample layer has out-of-plane
13 magnetization at zero-field.

14 Importantly, there is a factor of ~ 0.1 difference between the ratios $R_{asym}^{IP}/R_{tot}^{OP}$ obtained from the in-
15 plane data in Fig. 2(a) and $R_{cent}^{OP}/R_{tot}^{OP}$ obtained from the out-of-plane data from Fig. 2(b), both indicating
16 the fraction of the sample with out-of-plane magnetization. This implies that in the ‘forward’-graded sample,
17 there also is an intermediate magnetic layer having both in-plane and out-of-plane magnetic easy axes [27].
18 That is, the magnetization of such intermediate layer will contribute to R_{cent}^{OP} observed in the vertical field
19 sweep in Fig. 2(b) but will not contribute to R_{asym}^{IP} observed in the in-plane field scans shown in Fig. 2(a).
20 From these results, we argue that the ‘forward’ sample consists of *three* regions, one with a robust in-plane
21 easy axis, one with a robust out-of-plane easy axis, and one intermediate layer whose magnetization aligns
22 in-plane when the field is applied in-plane, and out-of-plane when the field is out-of-plane. Quantitatively,
23 our results then indicate that nearly 10 % of the sample (corresponding to the P-rich region near the top of
24 the layer, where tensile strain is the greatest) has a robust out-of-plane easy axis; the bottom 80 % of the

1 sample (i.e., the region with lower P concentration, where either compressive or low tensile strain occurs)
2 has a robust in-plane easy axis; and the remaining 10 % of the sample (presumed to be between these two
3 regions) corresponds to the intermediate layer.
4

5 B. Magnetic anisotropy of ‘reverse’-graded sample

6 In contrast to the ‘forward’ sample, the case of the ‘reverse’-grown specimen shows a single magnetic
7 anisotropy, regardless of the applied magnetic field directions, as shown in Figs. 2(c) and 2(d). The out-of-
8 plane data in Fig. 2(d) clearly shows an abrupt square single hysteresis with a minimal coercive field,
9 indicating a robust out-of-plane easy axis. The in-plane measurement data seen in Fig. 2(c) also shows a
10 single hysteresis, but the hysteresis is much broader, which requires explanation. Since there is no in-plane
11 easy axis in the case of this sample, to understand the width and shape of the hysteresis observed in the in-
12 plane measurements, we again must invoke the unintended slight tilt of the applied field, H_{ex} , relative to
13 the sample plane. The transition condition for the in-plane scan is $|H_z| = |H_{ex} \sin \delta| \approx |H_c|$, where H_z is
14 a small vertical component of H_{ex} due to the slight misalignment between H_{ex} and the sample plane; and
15 H_c is the coercive field of the sample. Since the field H_{ex} is applied near the film plane and the angle δ is
16 caused by the slight misalignment, the value of δ is very small. This requires a much larger H_{ex} in the in-
17 plane measurement than H_c observed in out-of-plane measurements to achieve magnetization reversal.
18 Importantly, the magnitudes of the Hall resistance at zero-field are the same for the in-plane and out-of-
19 plane field scans (i.e., R_{cent}^{IP} and R_{cent}^{OP}), as seen in Figs. 2(c) and 2(d), clearly indicating that the entire
20 sample behaves as a single magnetic domain with strong single out-of-plane anisotropy.
21

22 C. Magnetic Anisotropy Parameters of Graded Samples

23 As shown in earlier studies [28-30], a numerical description of the magnetic anisotropy of a magnetic
24 film can be conveniently determined by measuring and analyzing the angular dependence of the Hall
25 resistance. We now follow this procedure to obtain the values of magnetic anisotropy parameters for our

1 ‘forward’- and ‘reverse’-graded samples. The solid-circle and open-square data in Fig 3 show the Hall
 2 resistance results obtained by rotating the magnetic field with a fixed magnitude in the (001) and (110)
 3 planes, respectively. In the case of the ‘reverse’ sample (see Fig. 3(b)), only the out-of-plane angular
 4 dependence data (i.e., only for the field rotated in the (110) plane) was measured since there is no in-plane
 5 magnetic anisotropy in that sample. The strengths of the rotating magnetic fields were chosen to be
 6 sufficiently high to coherently rotate the magnetization of the films as the field is rotated.

7 The angular dependence of magnetization (and therefore of R_{xy}) can then be understood in terms of
 8 magnetic free energy E , given by [28,29]:

$$9 \quad \frac{E}{M} = -\frac{1}{16}H_{4\parallel}(3 - \cos 4\varphi) \sin^2 \theta - \frac{1}{4}H_{4\perp} \cos^4 \theta - \frac{1}{2}H_{2\parallel} \sin^2 \theta \sin^2 \varphi$$

$$10 \quad + \frac{1}{2}(4\pi M - H_{2\perp}) \cos^2 \theta - H[\cos \theta \cos \theta_H + \sin \theta \sin \theta_H \cos(\varphi - \varphi_H)], \quad (2)$$

11 where $H_{4\parallel}$ and $H_{4\perp}$ are the in-plane and out-of-plane components of cubic anisotropy field, and $H_{2\parallel}$ and
 12 $H_{2\perp}$ are the in-plane and the out-of-plane components of uniaxial anisotropy field. Since the magnetization
 13 of the film follows the free energy minima as the magnetization rotates, and the value of the Hall resistances
 14 depend directly on the direction of the magnetization, the angular dependence of the Hall resistances can
 15 be fitted by using the magnetic anisotropy fields shown in Eq. (2) as fitting parameters. For fitting the values,
 16 we adapted the magnetization value of 32 emu/cm³ obtained in an earlier study carried out on the samples
 17 with a similar Mn concentration [31]. The fitting process used here is described in detail in Ref. [30], and
 18 the results of the fitting are shown in Fig. 3.

19 The magnetic anisotropy parameters obtained by this analysis are summarized in Table I. Note that
 20 transport measurements probe the entire sample, rather than each of the layers separately. The magnetic
 21 anisotropy parameters obtained from these measurements thus represent the sample as a whole, even though
 22 the ‘forward’ sample consists of different sublayers having different magnetic free energies.

23 Table. I Magnetic anisotropy components of graded $\text{Ga}_{1-x}\text{Mn}_x\text{As}_{1-y}\text{P}_y$ samples

	$\mathbf{H}_{4\parallel}$ (G)	$\mathbf{H}_{4\perp}$ (G)	$\mathbf{H}_{2\parallel}$	$\mathbf{H}_{2\perp}$ (G)
‘Forward’	577.3	1600	-396.5	-1164
‘Reverse’	-	713	-	8008

1 3-D diagrams of magnetic free energy constructed using the fitting parameters in Table I are shown
2 in Figs. 4(a) and 4(b). Figure 4(b) clearly shows that the ‘reverse’ sample is described by a simple anisotropy
3 determined by only one vertical easy axis. In sharp contrast, the case of the ‘forward’ sample is much more
4 complex, consisting of coexisting distinct in-plane and out-of-plane anisotropies shown in Fig. 4(a) that
5 arise from contributions of the three sublayers comprising this sample, as discussed earlier. We plot the xy -
6 (i.e., the film-plane) and the yz - (i.e., the out-of-plane) cross-sectional profiles of magnetic free energy for
7 the ‘forward’ sample in Figs. 4(c) and 4(d). Figure 4(c) represents the in-plane anisotropy of the ‘forward’
8 sample, corresponding to the bottom and the intermediate sublayers. The two-fold symmetry of the in-plane
9 anisotropy imposed by the portion of the sample with in-plane easy axes is evident in the energy diagram
10 in Fig. 4(c).

11 The origins of the vertical cross-section (i.e., the yz -plane diagram) of the ‘forward’ sample shown
12 in Fig. 4(d) are more complex in that the energy profile for that case involves contributions of the sublayers
13 with the in-plane and the out-of-plane symmetries, along with that of the intermediate sublayer. Fortunately,
14 the contributions from each of the sublayers can be inferred from the ratios of the perpendicular-to-total
15 magnetization for each sublayer that have already been obtained from Fig. 2. We recall the weight factors
16 of 0.80, 0.10, and 0.10 obtained from the analysis of Fig. 2 for the bottom (in-plane easy axis), intermediate
17 (easy axes both in-plane and out-of-plane), and top sublayers (easy axis in out-of-plane direction),
18 respectively. The contributions from each of the sublayers to the total anisotropy are plotted as red, green,
19 and blue curves in Fig. 4(e). The sum of all three anisotropy diagrams, plotted as a black line in Fig. 4(e),
20 very nicely reproduces the energy contour obtained experimentally for the yz -plane shown in Fig. 4(d).

21

1 D. Temperature Dependence of Magnetic Anisotropy of Graded Samples

2 To obtain additional insights into the magnetic anisotropy of the graded $\text{Ga}_{1-x}\text{Mn}_x\text{As}_{1-y}\text{P}_y$ samples, we
3 have also studied the dependences of the Hall resistances on the temperature in our two specimens by
4 sweeping the magnetic field both in-plane and out-of-plane at several temperatures, as shown in Fig. 5. In
5 the case of the ‘forward’ sample (Figs. 5(a) and 5(b)), one can clearly see that the magnitude of the Hall
6 resistances for the in-plane and out-of-plane field scans decrease very rapidly with increasing temperature,
7 and nearly disappears at 40 K, close to the Curie temperature of the ‘forward’ sample.

8 The ‘reverse’ sample also shows a systematic decrease of the amplitude and the width of the
9 hysteresis in both in-plane and out-of-plane measurements as temperature increases (see Figs. 5(c) and 5(d)).
10 This behavior is typical for a ferromagnetic layer with perpendicular anisotropy. However, note that a two-
11 step transition behavior becomes evident in these measurements at 50 K and disappears again above 60 K
12 in Figs. 5(c) and 5(d). We interpret this as an indication that the ‘reverse’ sample is also divided into two
13 magnetically different regions with out-of-plane anisotropy but with different Curie temperatures. That is,
14 even though the ‘reverse’ sample shows a simple single-domain behavior at low temperature, the coercive
15 field in different fractions of the layer exhibits different rates of decrease with the temperature (presumably
16 due to different phosphorus content due to grading), the difference becoming conspicuous around 40 K.
17 However, since one fraction of the film reaches the Curie temperature first, above 60 K, the behavior returns
18 to a single-hysteresis behavior.

19 IV. Discussions

20 The results described above are rather unexpected. First, since the gradation of phosphorus in both
21 samples is very similar and the strain is not relaxed in the two samples, one would expect them to have
22 approximately similar distributions of in-plane and out-of-plane magnetizations, albeit along opposite
23 directions. And second, both samples contain more layers with tensile than compressive strain, and thus
24 one would expect that both will have a larger fraction of sublayers with perpendicular than with in-plane
25

1 anisotropy. Surprisingly, however, neither of these expectations is true. As has been shown, the forward
2 sample is dominated in a ratio of about 8:1 by magnetic in-plane anisotropy, while in the reverse sample
3 the effect of in-plane anisotropy is entirely eliminated. In the following discussion, we attempt to explain
4 these unexpected results.

5 Let us first consider the forward sample. We know that the top of the valence band of GaP lies
6 approximately 400 meV lower in the energy than in GaMnAs. We therefore expect that as the phosphorus
7 concentration is increased in each additional layer of our graded GaMnAsP sample, the top of the valence
8 band will move progressively downward by a few meV relative to the preceding layer, as schematically
9 indicated in Fig. 6(a). This will lead to interesting growth dynamics in such a graded system, as discussed
10 below, and will have an important effect on the properties of the resulting specimen.

11 Consider the first ($y = 0.03$) sublayer 1 in Fig. 6(a). When it is grown, it will have a certain
12 concentration x_{sub} of Mn ions substitutionally occupying Ga sites, and a certain concentration of Mn
13 interstitials x_i characteristic for the growth conditions used. We recall that the substitutional incorporation
14 of Mn at Ga sites is limited by the Fermi energy, as discussed in Yu *et al.* [32], resulting in the formation
15 of Mn interstitials when the concentration of holes due to x_{sub} exceeds a certain limit. Now, as we deposit
16 sublayer 2 ($y = 0.05$ in Fig. 6(a)) on sublayer 1, the small but finite band offset between the two layers will
17 become important. Like in the modulation doping experiments of Wojtowicz *et al.* [33], some holes will
18 be siphoned off into sublayer 1 due to the band offset between the layers. This lowers the Fermi energy in
19 sublayer 2, allowing x_{sub} to increase, and reducing x_i formed in this layer. We now recall that the number
20 of active magnetic moments in a given layer is proportional to $x_{\text{eff}} = x_{\text{sub}} - x_i$, and the number of holes is
21 determined by $x_p = x_{\text{sub}} - 2x_i$ [21], indicating that magnetization M of sublayer 2 will be more robust
22 than in sublayer 1 due to the increase in x_{sub} and the reduction of x_i . Similarly, as sublayer 3 is being grown,
23 the holes produced by substitutional incorporation of Mn are siphoned off to the preceding layer(s), again
24 allowing a higher substitutional and lower interstitial incorporation of Mn, and leading to a greater
25 magnitude of M . We can now make the same argument for sublayer 4, 5, etc.: as each successive layer is

1 grown, holes are drained off to the preceding layer(s), allowing the growing layer to end up with larger
2 substitutional incorporation of Mn at Ga sites, and consequently a lower concentration of the harmful
3 mobile interstitials.

4 While this process would appear to lead to increased magnetization in successive layers, there are
5 important trade-offs that must be considered. As each new layer is grown, the holes themselves – of key
6 importance to the ferromagnetism of the material – are drained off to layers grown earlier. It is likely that,
7 as the number of layers already grown increases, the "sink" for these holes becomes increasingly more
8 effective, in analogy to modulation doping experiments, where it was shown that the effect of a doped
9 barrier in modulation doping is proportional to its width [34]. Additionally, in this case one needs to
10 consider the effect of increasing phosphorus concentration on the magnetization in successive layers of the
11 "forward" sample. It has been shown by Dong, *et al.* [21] that increasing phosphorus concentration leads to
12 increased localization of holes, which automatically reduces magnetization. Based on these trade-offs, it
13 appears likely that the center of gravity of magnetization in the multilayer would naturally occur somewhere
14 in the middle layers. However, at this time, we cannot meaningfully discuss just where in the multilayer
15 this takes place.

16 This interpretation appears quite consistent with the data shown in Fig. 2, which indicate that the
17 forward sample as a whole is described by 80 % to 90 % of in-plane magnetization. At first glance this
18 behavior would be surprising, since not more than three layers of the sample correspond to strain conditions
19 that favor in-plane magnetic anisotropy, while the remaining five layers favor perpendicular magnetization.
20 However, the picture presented above explains this quite nicely, despite its qualitative nature. As new layers
21 are grown, the concentration of holes in the lower layers (i.e., those favoring in-plane anisotropy) increases
22 both through hole drainage from layers grown later and (except for sublayer 1) through a lower rate of
23 formation of Mn interstitials. These processes result in a disproportional increase of magnetization in the
24 lower layers, consistent with the observed anisotropy of magnetization.

1 We now consider the "reverse" sample, again starting with the first ($y = 0.24$) layer illustrated by
2 Fig. 6(b). When it was grown, this layer had concentrations x_{sub} and x_i consistent with the low-temperature
3 MBE growth conditions used, so that the effective Mn spin concentration in the layer is given by x_{eff} , and
4 the hole concentration is proportional to x_p defined earlier. When the second ($y = 0.19$) layer is deposited,
5 because of the band offset shown in Fig. 6(b), some holes are siphoned from the first layer into this sublayer
6 2 as its growth takes place. (We note parenthetically: In the forward sample, holes were drained away from
7 the sample being grown. In the reverse case, they were siphoned into the growing sample.) This does not
8 affect the interstitials in the first layer since that layer is already grown; but in sublayer 2, the presence of
9 additional holes now inhibits Mn substitution at Ga sites, thus causing more interstitials to form. So, in
10 sublayer 2, we now have a reduced number of active Mn moments and also significantly fewer holes formed
11 (both due to the lower rate of formation of x_{sub} , and due to compensation by Mn interstitials x_i whose rate
12 of formation is increased). The same argument can now be applied to sublayers 3, 4, etc. So, as P decreases
13 in successive layers, moving the top of the valence band to higher energy with each successive layer, more
14 interstitials will form in the new layers, reducing substitutional incorporation of Mn, and thus successively
15 reducing their magnetization. It must be emphasized that the deleterious effect of interstitials on
16 magnetization is very strong, and can exceed the beneficial effect of holes entering the layer, as has been
17 strikingly demonstrated in co-doping experiments of Lee *et al.* [35], who showed that adding holes to
18 GaMnAs by additional doping results (counter-intuitively) in a reduction rather than an increase of
19 magnetization. The large influx of holes into uppermost layers from the rest of the sample may thus prevent
20 substitutional incorporation of Mn to such a degree that magnetization of those layers will be substantially
21 reduced, or will even vanish altogether. As a result, the magnetization of the reverse graded sample is also
22 dominated by the bottom layers, which in this case favor perpendicular magnetic anisotropy, consistent
23 with the observed orientation of magnetization in this specimen.

24

25

V. Conclusions

1 Magnetic anisotropy of $\text{Ga}_{1-x}\text{Mn}_x\text{As}_{1-y}\text{P}_y$ samples with graded phosphorus concentration
2 shows distinct differences between ‘forward’- and ‘reverse’-graded specimens, even though the P
3 concentration y varies over a similar range (i.e., from about $y \approx 0$ to $y \approx 0.25$) in both films. Most
4 of the ‘forward’-graded sample is strongly dominated by in-plane easy axes of magnetization,
5 while the ‘reverse’-graded specimen exhibits only out-of-plane magnetization. This indicates,
6 surprisingly, that growth dynamics of graded the $\text{Ga}_{1-x}\text{Mn}_x\text{As}_{1-y}\text{P}_y$ film predetermines the magnetic
7 properties of the entire film, despite the graded composition profile of the sample. While these
8 results by themselves already provide helpful information for engineering magnetic anisotropy in
9 ferromagnetic $\text{Ga}_{1-x}\text{Mn}_x\text{As}_{1-y}\text{P}_y$ films by gradual variation of the phosphorus content during growth,
10 the observed behavior is quite unexpected and requires further study to understand its physical
11 origins.

12

13

ACKNOWLEDGEMENTS

14 This research was supported by Basic Science Research Program through the National Research
15 Foundation of Korea (NRF) funded by the Ministry of Education (2018R1D1A1A02042965); by Basic
16 Science Research Program through the NRF of Korea (2021R1A2C1003338); by Ministry of Science ICT
17 (2018R1A4A1024157); by the NRF under the BK21 FOUR program at Korea University, Initiative for
18 science frontiers on upcoming challenges; by Korea University Grant; and by National Science Foundation
19 Grant DMR 1905277.

References

- 1
- 2 [1] H. Ohno, *Science* **281**, 951 (1998).
- 3 [2] T. Dietl and H. Ohno, *Rev. Mod. Phys.* **86**, 187 (2014).
- 4 [3] T. Dietl, H. Ohno, F. Matsukura, J. Cibert, and D. Ferrand, *Science* **287**, 1019 (2000).
- 5 [4] M. Abolfath, T. Jungwirth, J. Brum, and A. H. MacDonald, *Phys. Rev. B* **63**, 054418 (2001).
- 6 [5] M. Sawicki, F. Matsukura, A. Idziaszek, T. Dietl, G. M. Schott, C. Ruester, C. Gould, G.
7 Karczewski, G. Schmidt, and L. W. Molenkamp, *Phys. Rev. B* **70**, 245325 (2004).
- 8 [6] A. Shen, H. Ohno, F. Matsukura, Y. Sugawara, N. Akiba, T. Kuroiwa, A. Oiwa, A. Endo, S.
9 Katsumoto, and Y. Iye, *J. Cryst. Growth* **175-176**, 1069 (1997).
- 10 [7] H. Lee, J. Chang, P. Chongthanaphisut, S. Lee, S. Choi, S.-K. Bac, A. R. Nasir, S. Lee, A. Pardo,
11 S. Dong, X. Li, X. Liu, J. K. Furdyna, and M. Dobrowolska, *AIP Adv.* **7**, 055809 (2017).
- 12 [8] J. Chang, S. Choi, K. Lee, S.-K. Bac, S. Choi, P. Chongthanaphisut, S. Lee, X. Liu, M.
13 Dobrowolska, and J. K. Furdyna, *J. Cryst. Growth* **512**, 112 (2019).
- 14 [9] M. Cubukcu, H. J. von Bardeleben, K. Khazen, J. L. Cantin, O. Mauguin, L. Largeau, and A.
15 Lemaître, *Phys. Rev. B* **81**, 041202(R) (2010).
- 16 [10] A. Lemaître, A. Miard, L. Travers, O. Mauguin, L. Largeau, C. Gourdon, V. Jeudy, M. Tran, and
17 J.-M. George, *Appl. Phys. Lett.* **93**, 021123 (2008).
- 18 [11] M. L. Lee, E. A. Fitzgerald, M. T. Bultsara, M. T. Currie, and A. Lochtefeld, *J. Appl. Phys.* **97**,
19 011101 (2005).
- 20 [12] C.-Z. Ning, L. Dou, and P. Yang, *Nat. Rev. Mater.* **2**, 17070 (2017).
- 21 [13] A. Werpachowska and T. Dietl, *Phys. Rev. B* **82**, 085204 (2010).
- 22 [14] T. Gora and F. Williams, *Phys. Rev.* **177**, 1179 (1969).
- 23 [15] V. K. Vlasko-Vlasov, W. K. Kwok, S. Dong, X. Liu, M. Dobrowolska, and J. K. Furdyna, *Phys.*
24 *Rev. B* **98**, 180411(R) (2018).

- 1 [16] S. Dong, Y.-L. Wang, S.-K. Bac, X. Liu, V. Vlasko-Vlasov, W.-K. Kwok, S. Rouvimov, S. Lee,
2 M. Dobrowolska, and J. K. Furdyna, *Phys. Rev. Mater.* **3**, 074407 (2019).
- 3 [17] T. Niazi, M. Cormier, D. Lucot, L. Largeau, V. Jeudy, J. Cibert, and A. Lemaître, *Appl. Phys.*
4 *Lett.* **102**, 122403 (2013).
- 5 [18] M. Cormier, V. Jeudy, T. Niazi, D. Lucot, M. Granada, J. Cibert, and A. Lemaître, *Phys. Rev. B*
6 **90**, 174418 (2014).
- 7 [19] S.-H. C. Baek, V. P. Amin, Y.-W. Oh, G. Go, S.-J. Lee, G.-H. Lee, K.-J. Kim, M. D. Stiles, B.-G.
8 Park, and K.-J. Lee, *Nat. Mater.* **17**, 509 (2018).
- 9 [20] K. M. Yu, W. Walukiewicz, T. Wojtowicz, W. L. Lim, X. Liu, U. Bindley, M. Dobrowolska, and
10 J. K. Furdyna, *Phys. Rev. B* **68**, 041308(R) (2003).
- 11 [21] S. Dong, L. Riney, X. Liu, L. Guo, R.-K. Zheng, X. Li, S.-K. Bac, J. Kossut, M. Dobrowolska, B.
12 Assaf, and J. K. Furdyna, *Phys. Rev. Mater.* **5**, 014402 (2021).
- 13 [22] See Supplemental Material at [URL here] for a description of structural information and details of
14 Arrott plot analysis.
- 15 [23] K. Okamoto, *J. Magn. Magn. Mater.* **35**, 353 (1983).
- 16 [24] H. X. Tang, S. Masmanidis, R. K. Kawakami, D. D. Awschalom, and M. L. Roukes, *Nature* **431**,
17 52 (2004).
- 18 [25] W. L. Lim, X. Liu, K. Dziatkowski, Z. Ge, S. Shen, J. K. Furdyna, and M. Dobrowolska, *Phys.*
19 *Rev. B* **74**, 045303 (2006).
- 20 [26] T. Yoo, S. Khym, S.-Y. Yea, S. Chung, S. Lee, X. Liu, and J. K. Furdyna, *Appl. Phys. Lett.* **95**,
21 202505 (2009).
- 22 [27] M. Yahyaoui, C. Testelin, C. Gourdon, and K. Boujdaria, *J. Appl. Phys.* **111**, 033902 (2012).
- 23 [28] M. Farle, *Rep. Prog. Phys.* **61**, 755 (1998).
- 24 [29] X. Liu, W. L. Lim, L. V. Titova, M. Dobrowolska, J. K. Furdyna, M. Kutrowski, and T.
25 Wojtowicz, *J. Appl. Phys.* **98**, 063904 (2005).

- 1 [30] H. Son, S. Chung, S.-Y. Yea, S. Lee, X. Liu, and J. K. Furdyna, *J. Appl. Phys.* **103**, 07F313
2 (2008).
- 3 [31] X. Li, X. Liu, S. Dong, C. Gorsak, J. K. Furdyna, M. Dobrowolska, S.-K. Bac, S. Lee, and S.
4 Rouvimov, *J. Vac. Sci. Technol. B* **36**, 02D104 (2018).
- 5 [32] K. M. Yu, W. Walukiewicz, T. Wojtowicz, I. Kuryliszyn, X. Liu, Y. Sasaki, and J. K. Furdyna,
6 *Phys. Rev. B* **65**, 201303(R) (2002).
- 7 [33] T. Wojtowicz, W. L. Lim, X. Liu, M. Dobrowolska, J. K. Furdyna, K. M. Yu, W. Walukiewicz, I.
8 Vurgaftman, and J. R. Meyer, *Appl. Phys. Lett.* **83**, 4220 (2003).
- 9 [34] K. M. Yu, T. Wojtowicz, W. Walukiewicz, X. Liu, and J. K. Furdyna, in *Semiconductors and*
10 *Semimetals*, edited by E. R. Weber (Elsevier, 2008), pp. 89.
- 11 [35] S. Lee, S. J. Chung, I. S. Choi, S. U. Yuldeshev, H. Im, T. W. Kang, W.-L. Lim, Y. Sasaki, X.
12 Liu, T. Wojtowicz, and J. K. Furdyna, *J. Appl. Phys.* **93**, 8307 (2003).

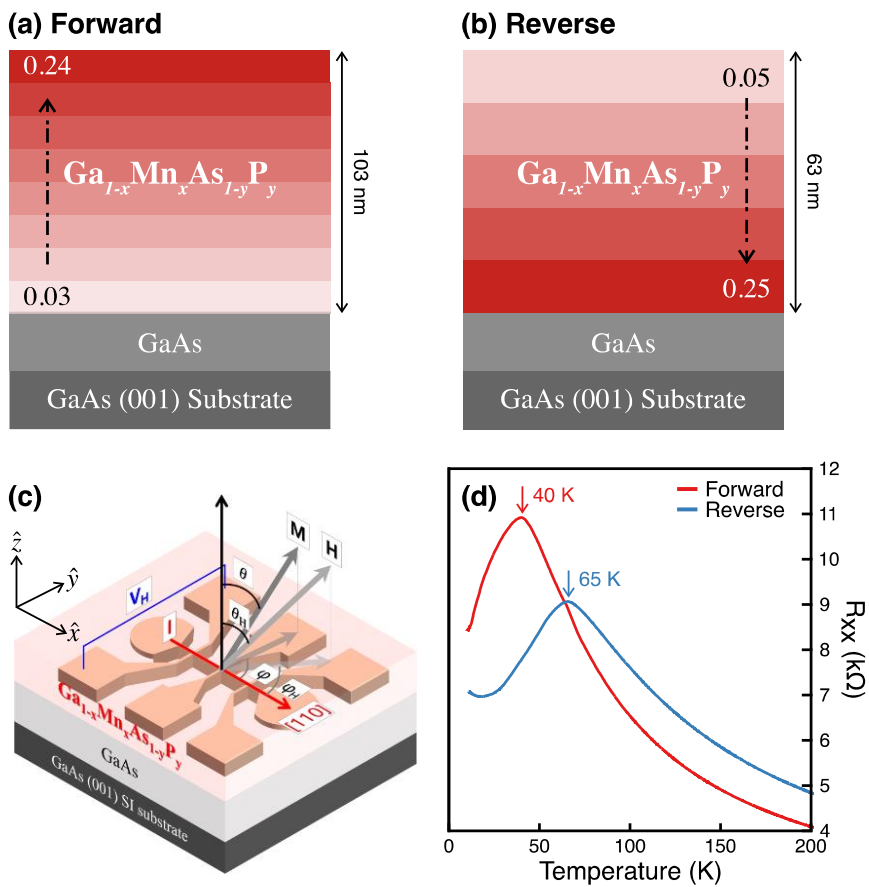
13

Figures

1

2 Figure 1.

3 Sketch of the structures for (a) ‘forward’- and (b) ‘reverse’-graded $\text{Ga}_{1-x}\text{Mn}_x\text{As}_{1-y}\text{P}_y$ samples. Chemical
 4 compositions and the thicknesses shown in the figures for each sample were obtained by XRD
 5 measurements. (c) Schematic diagram of the Hall bar patterned on the graded $\text{Ga}_{1-x}\text{Mn}_x\text{As}_{1-y}\text{P}_y$ film,
 6 indicating Hall voltage V_H , and directions of the current I , magnetization M , and external field H . Current
 7 I flows along the [110] crystallographic direction. (d) Temperature dependences of resistances measured
 8 for the ‘forward’ (red) and ‘reverse’ (blue) samples.



9

1 Figure 2.

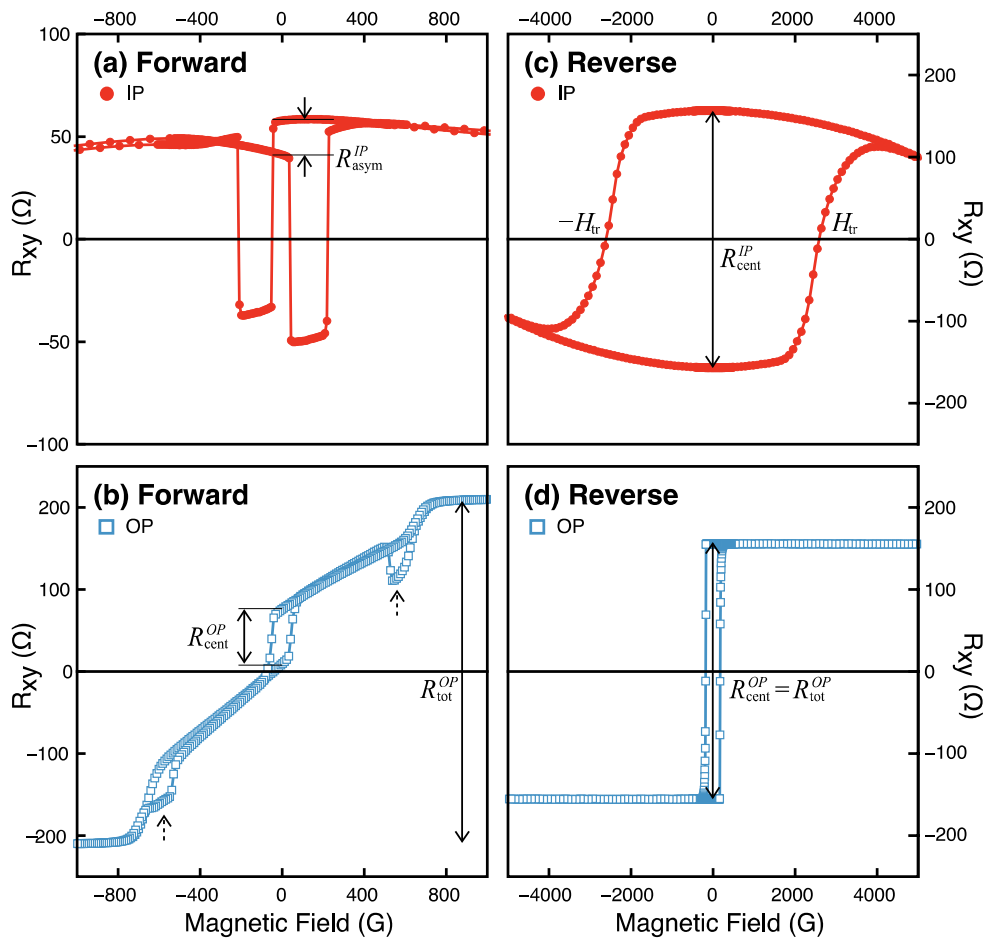
2 Hall resistance R_{xy} obtained by sweeping magnetic field in-plane (top row) and out-of-plane (bottom row)

3 for ‘forward’ (a and b) and ‘reverse’ (c and d) samples at 10 K. R_{asym}^{IP} and R_{cent}^{OP} are differences of Hall

4 resistance at zero-field between up- and down-field scans in in-plane and out-of-plane data. R_{tot}^{OP} represents

5 a maximum change of the anomalous Hall resistance for out-of-plane field scan. H_{tr} in (c) indicate

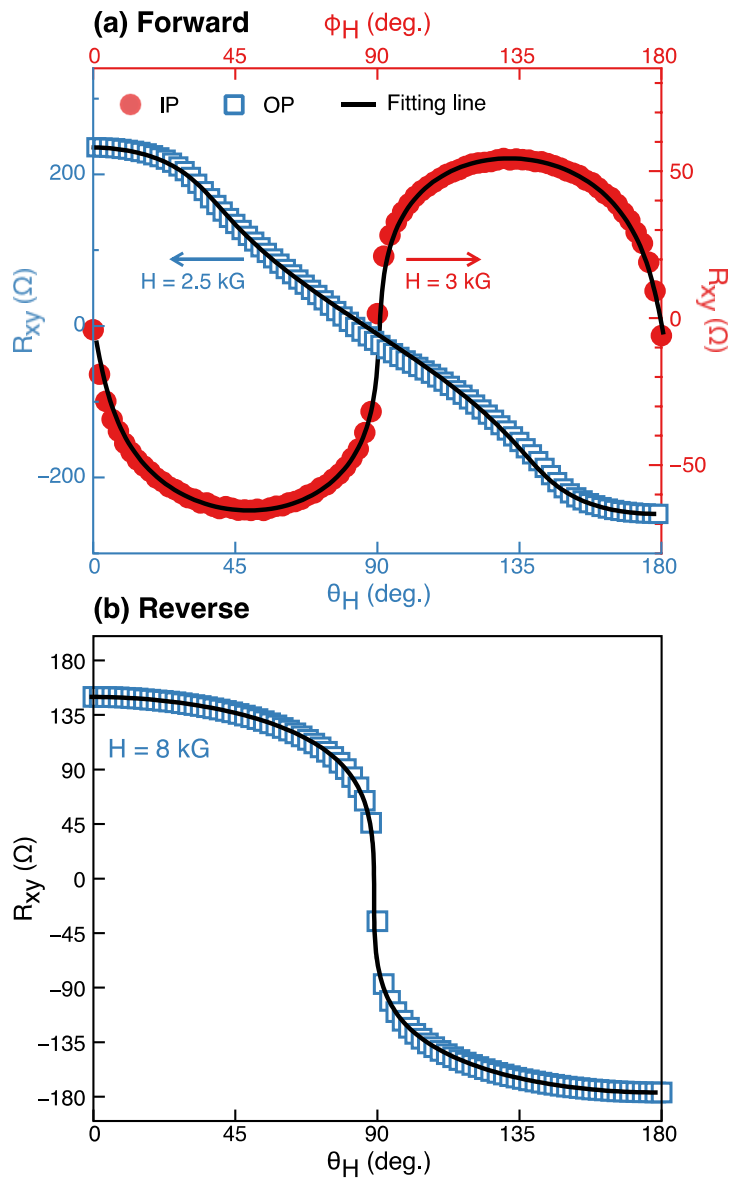
6 transition fields in in-plane field scan for the ‘reverse’ sample.



7

1 Figure 3.

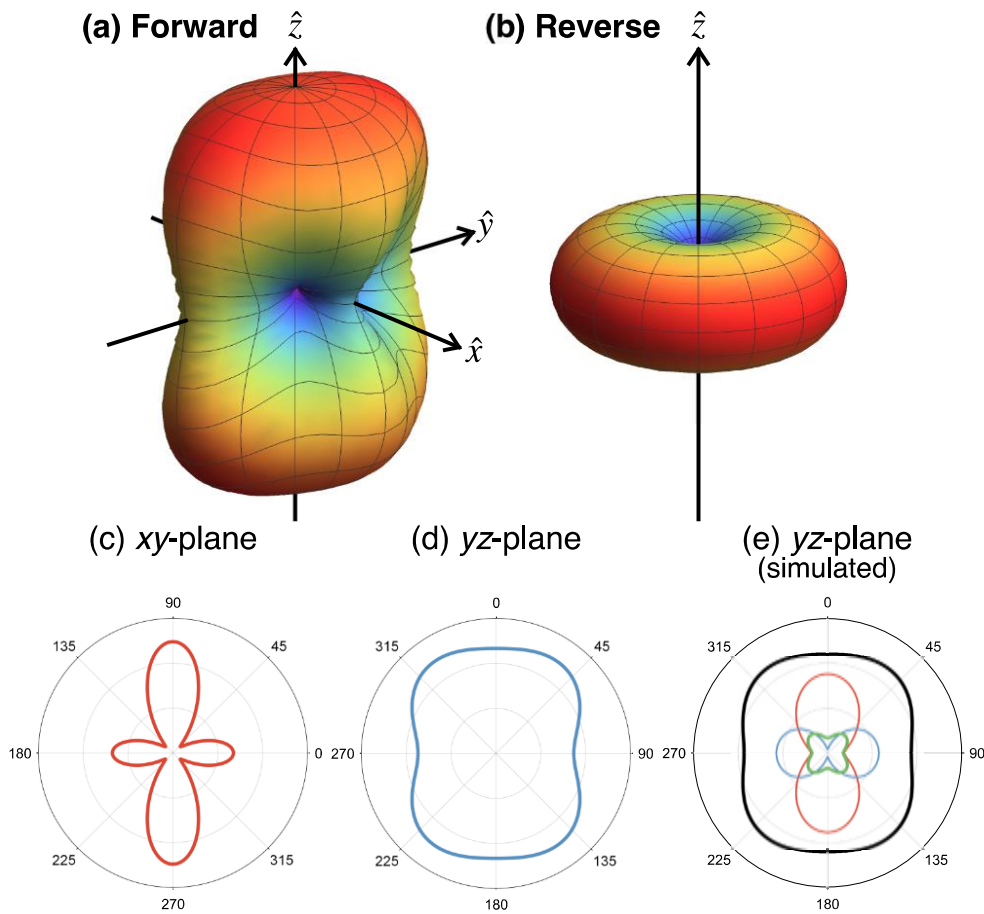
2 Angular dependence of Hall resistance measured at 5 K for (a) 'forward' and (b) 'reverse' samples. Solid
3 circles represent data obtained by rotating the field within the film plane (i.e., the (001) plane, referred to
4 as xy -plane); and open squares are obtained with field rotated out-of-plane (i.e., in the (110) plane, referred
5 to as yz -plane). Black solid curves are fitting results obtained using magnetic free energy anisotropy field
6 parameters discussed in the text.



7

1 Figure 4.

2 Three-dimensional (3-D) polar plots of magnetic free energy density for (a) 'forward' and (b) 'reverse'
3 samples. Cross-sectional 2D plots for the xy -plane and the yz -plane for the 'forward' sample are shown in
4 panels (c) and (d), respectively. (e) The red, green, and blue lines represented magnetic anisotropies for the
5 bottom, middle, and top sublayers of the 'forward' sample, respectively. The black curve in (e) is the free
6 energy contour obtained by summing magnetic anisotropy contributions of the three magnetic sublayers
7 using the ratios obtained from Fig. 2.

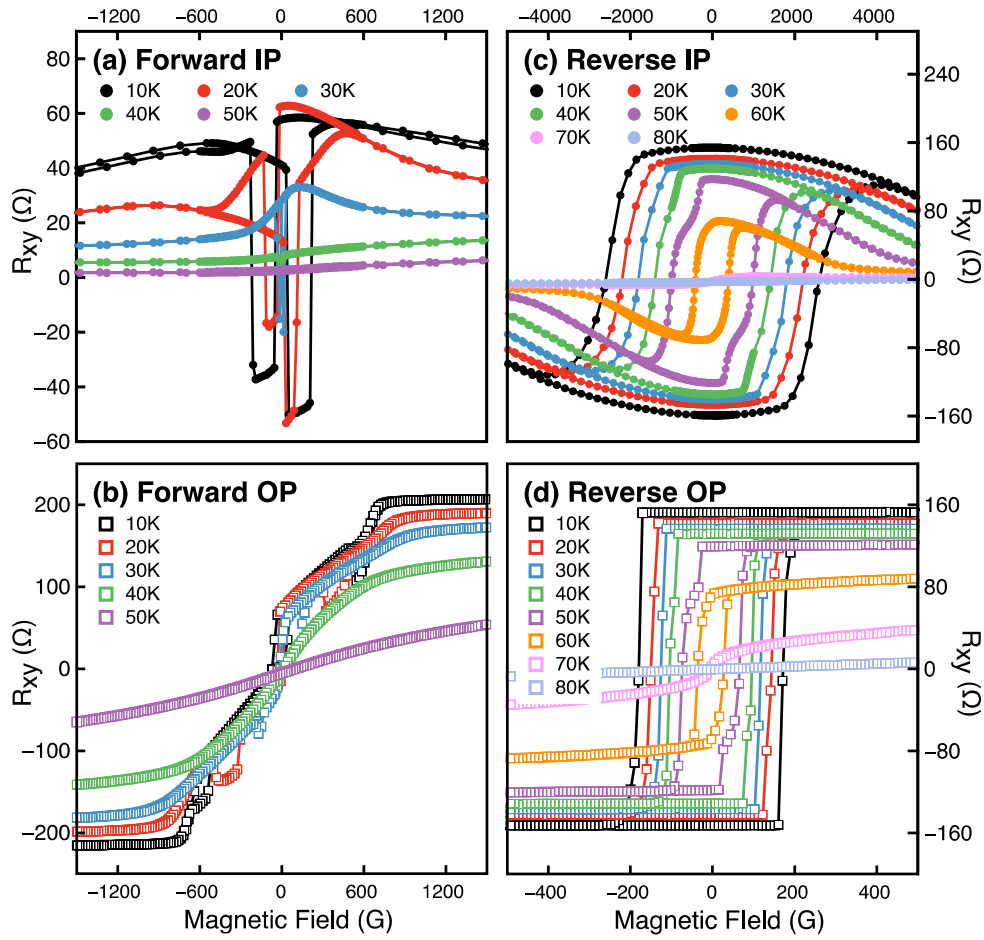


8

1 Figure 5.

2 Hall resistances R_{xy} obtained by sweeping magnetic field along in-plane (top row) and out-of-plane

3 (bottom row) directions for ‘forward’ and ‘reverse’ samples at several temperatures.



4

- 1 Figure 6.
- 2 Schematic band structure of forward (a) and reverse (b) samples. Blue lines mark each top of the valence
- 3 band (VB) in successive sublayers. Chemical compositions shown in the figures for each sublayer
- 4 were obtained by XRD measurements.

